



**POLITECNICO**  
MILANO 1863

**[RE.PUBLIC@POLIMI](#)**

Research Publications at Politecnico di Milano

## Post-Print

This is the accepted version of:

M. Belan, F. Messanelli

*Compared Ionic Wind Measurements on Multi-Tip Corona and Dbd Plasma Actuators*

Journal of Electrostatics, Vol. 76, 2015, p. 278-287

doi:10.1016/j.elstat.2015.06.008

The final publication is available at <https://doi.org/10.1016/j.elstat.2015.06.008>

Access to the published version may require subscription.

**When citing this work, cite the original published paper.**

© 2015. This manuscript version is made available under the CC-BY-NC-ND 4.0 license

<http://creativecommons.org/licenses/by-nc-nd/4.0/>

Permanent link to this version

<http://hdl.handle.net/11311/962038>

# Compared ionic wind measurements on multi-tip corona and DBD plasma actuators

Marco Belan, Federico Messanelli

Politecnico di Milano, Dipartimento di Scienze e Tecnologie Aerospaziali, via La Masa 34, 20156 Milano, Italia

## Abstract

Two sets of actuators with triangular tips on their active electrodes (13 corona and 15 DBD) are studied in the laboratory. Far field ionic wind velocity, mass flow and efficiency are measured for all the actuators. The best electrode shape as function of tip sharpness and tips number/unit length is determined for each of the above measurements. The gas velocity increases downstream of the tips in all the actuators, but the DBD flow has a three-dimensional structure more complicated than for coronas. The tips improve the efficiency of all the actuators, and the stability of coronas is remarkably improved.

Keywords: Plasma actuator geometry – Corona actuator – DBD actuator – Flow control

## 1 Introduction

The plasma actuators are widely studied because of their ability to produce a ionic wind, that can be used for several flow control purposes. For the most part, the actuators belong to the categories of corona and DBD, the former DC-driven and the latter AC-driven. The properties of these actuators are widely discussed in the review of Moreau [1], and specifically for the DBD by Corke et al. [2], Wang et al. [3] and Benard and Moreau [4]. The resulting ionic wind velocity is a crucial parameter in defining the performance of a given actuator, and it can be influenced in many ways, acting on electrodes gap, size, shape and arrangement in general, and for the DBD on the dielectric material and size as well as on the waveform.

The shape of the electrodes seems to be a very important parameter: actually, it is known that the modification of one or both the electrodes in a DBD from the standard straight shape toward periodic sinuous, triangular or square shapes has remarkable effects. Sharp tips increase ionic wind and thrust [5, 6], and in general all these shapes may induce transverse velocity components that lead to three-dimensional flows in the near field and finally to the creation of streamwise vortex structures [3, 7], useful for the boundary layer control when the actuator interacts with an external stream.

The present work is focused on the effects of the electrodes geometry, and in particular on the effects of multiple tips on the edge of an electrode. Up to now, multiple tips and triangular patterns known as 'serrated geometry' have been studied in the laboratory by few authors and only for some specific cases of DBD actuators, as for example in Ref. [5, 6, 8, 9].

In this experiment, several DBD and corona actuators with triangular tips are considered. Their multi-tip electrodes are the exposed pole for the DBD and the anodic pole for the corona (upstream electrodes). Within the corona and DBD sets, each actuator is identified by the height/width ratio of the tips and by the tips number per unit length. The aim of the work is to draw some general properties of the geometry under study, but a serious limit is set by the complex characterization of an actuator, that may require several tests. Actually, the complete description of a single multi-tip device could require electric measurements as well as fluid dynamic measurements, for example PIV maps for the 3D motion in

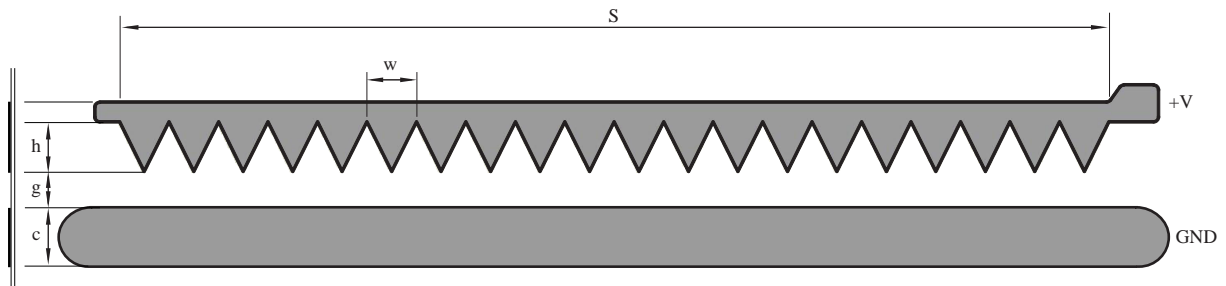


Figure 1: Common geometry for the corona actuators; the section is shown on the left side. Gap  $g = 15\text{mm}$  and cathode size  $c = 24\text{mm}$  for all the actuators.

the near field of the tips, ionic wind velocity in the far field, thrust measurements, effects of the actuator on a given body in a wind tunnel, and so on. However, the number of different actuators considered in this work, which amounts to 28, imposes the selection of a representative test in order to carry out experimental comparisons in a reasonable time. For this reason, and considering the differences between corona and DBD, in the present study the comparisons are carried out on the basis of the far field ionic wind velocity, measured on different planes normal to the main direction of the stream. In this regard, the dependence of the induced longitudinal velocity on the tips of the exposed electrodes has been shown at least in a particular case of DBD [9].

The chance of testing several corona actuators is per se another remarkable point of this investigation. Actually, the present study has also evidenced that the stability of corona actuators increases with the sharpness of the tips, making them more manageable than the standard straight wire-to-plate, quite subject to sparks and possibly arc transitions [10, 11].

## 2 Experimental setup

Size and geometries of the actuators under study have been selected after dimensional considerations and preliminary tests in such a way as to obtain results in the same magnitude order, comparable within each set (corona and DBD) and possibly between different sets.

The geometry common to the 13 corona actuators is shown in Fig. 1 and the one for the 15 DBD actuators under test is shown in Fig. 2. All the actuators have a working span  $S = 400\text{mm}$  in order to include a sufficient number of tips and reduce the end effects in the measurements, with the exception of the straight corona (wire-to-plate), which is shorter because of its poor stability as explained below. The tip-to-cathode gap of the coronas is always  $g = 15\text{mm}$ , the cathode size as in figure is always  $c = 24\text{mm}$ . The immersed (grounded) electrode for the DBDs is always aligned with the roots of the exposed electrode, its size  $c = 50\text{mm}$  is long enough to permit the complete development of the plasma sheet over all the actuators. All the electrodes are made of aluminum tape,  $0.12\text{mm}$  thick, except the straight corona anode, which is a copper wire with a diameter of  $0.1\text{mm}$ . The supporting plate is made of plexiglas,  $2\text{mm}$  thick, the same material acts as a dielectric for the DBD actuators, where the immersed electrode is also encapsulated in epoxy resin to prevent unwanted plasma formation. The multi-tip electrodes, i.e. the anode for the corona and the exposed one for the DBD, are parameterized by means of the tips height  $h$ , width  $w$  and number  $N$ .

The complete sets of electrodes under test are shown in Fig. 3 and 4 for the two kinds of actuators. These figures include parameterization tables, where each electrode is labeled by its  $h$  and  $w$  values, together with their ratio  $h/w$  (tip sharpness) and the number of tips per unit length. The last two

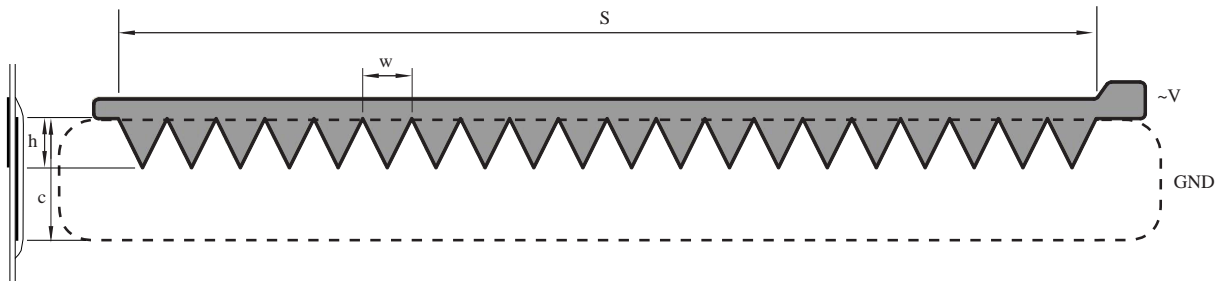


Figure 2: Common geometry for the DBD actuators; the section is shown on the left side (ground electrode encapsulated in epoxy resin). Ground electrode size  $c = 50\text{mm}$  for all the actuators.

quantities are also useful to define a parameter space

$$(n, r) = \left( \frac{N}{S}, \frac{h}{w} \right) \quad (1)$$

in order to present and discuss the results, including the dependence of the actuators performance on the  $h/w$  ratio, which has already been highlighted for the actuators characterization in other works [6, 8, 9]. The other parameter represents the periodicity of the electrode, since  $N/S = 1/\text{wavelength} = \text{wavenumber}/(2\pi)$ . The overall field of interest is approximately  $20 < n < 250$ ,  $0 < r < 5$ . Within each set, the choice of the actuators has been made in such a way as to cover suitable regions of interest, considering the preliminary tests and some expected results. In each set, 8 actuators have upstream electrodes identical to the corresponding ones in the other set, this permits some direct comparisons between the behaviours of an electrode in the two kinds of actuator. As references, each set includes a straight actuator without tips. The straight corona actuator is sketched over the same span as the others, but the real device under test is much shorter ( $S = 35\text{mm}$ ), because of its poor stability. Actually, at least a case of straight corona actuator  $400\text{mm}$  wide is known in literature [12], but in that case it was used in a wind tunnel, taking advantage of the known stabilizing effect of the airstream. In the present study instead the straight actuator is operated in still air, remarkably increasing the stability problems.

The corona actuators are driven by means of a suitable high voltage power supply unit, capable of  $6\text{mA}$  at  $V_0 = 20\text{kV}$  (Fig. 5). This PSU is equipped with a safety circuit that turns the power off when detects a spark: for this reason, the connection to the actuators has been implemented by means of a filter that simplifies the operations avoiding undesired power breakdowns ( $R = 4.4\text{M}\Omega$ ,  $C = 0.9\text{nF}$ ). As usual, the circuit includes a ballast resistor, in this case  $R_b = 4.4\text{M}\Omega$ . Voltage and current measurements are obtained by means of a 1:1000 voltage divider (load  $47\text{M}\Omega$ ) and a shunt resistor ( $R_s = 100\Omega$ ) on the ground electrode. All measurements have been carried out at  $V_0 = 17.2 \pm 0.2\text{ kV}$ , except the wire-plate case, that requires  $V_0 = 16 \pm 0.1\text{ kV}$  to ignite correctly with the same gap width  $g$  as the other actuators. As shown in the results section, this working point keeps the actuators in the streamer regime.

The DBD actuators are driven by a system purposely built, consisting of an oscillator, a power amplifier and an output transformer  $T$ , as sketched in Fig. 6. The system output can provide up to  $100\text{W}$  at  $20\text{kV}_{pp}$  (peak-to-peak, sinusoidal waveform). The measurement section is the same as for corona actuators. All measurements have been carried out at  $V_{pp} = 20 \pm 0.5\text{ kV}$  with frequency  $f = 815 \pm 5\text{ Hz}$ . This frequency has been identified as an optimal working point, close to the resonance condition [13] for all the actuators of the set. In fact, deviations in the order of  $\pm 200\text{ Hz}$  from this frequency, keeping each actuator at the same power level, lead in several tests to an increase of the input power needed by the driver, thus to a decrease of the electrical efficiency.

All the voltage and current waveforms have been acquired recording the output signals  $V = V_{out}(t)$ ,  $I = I_{out}(t)$  of Fig. 5 and 6 at sampling frequencies of  $100\text{Msamples/s}$ . The overall effect of the error





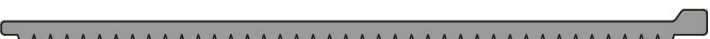







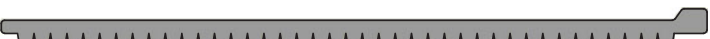
Geometry	h [mm]	w [mm]	h/w	N/S [m <sup>-1</sup> ]
C1 	0	---	0	---
C2 	8	4	2	250
C3 	8	5	1.6	200
C4 	10	10	1	100
C5 	15	10	1.5	100
C6 	20	4	5	250
C7 	20	5	4	200
C8 	20	8	2.5	125
C9 	20	10	2	100
C10 	20	20	1	50
C11 	30	10	3	100
C12 	40	10	4	100
C13 	40	10	4	50

Figure 3: Set of corona anodes under test.
















Geometry	h [mm]	w [mm]	h/w	N/S [m <sup>-1</sup> ]
D1 	0	---	0	---
D2 	3	10	0.3	100
D3 	5	5	1	200
D4 	5	10	0.5	100
D5 	10	10	1	100
D6 	15	10	1.5	100
D7 	20	5	4	200
D8 	20	10	2	100
D9 	20	20	1	50
D10 	20	25	0.8	40
D11 	20	40	0.5	25
D12 	25	10	2.5	100
D13 	30	10	3	100
D14 	35	10	3.5	100
D15 	40	10	4	50

Figure 4: Set of DBD exposed electrodes under test.

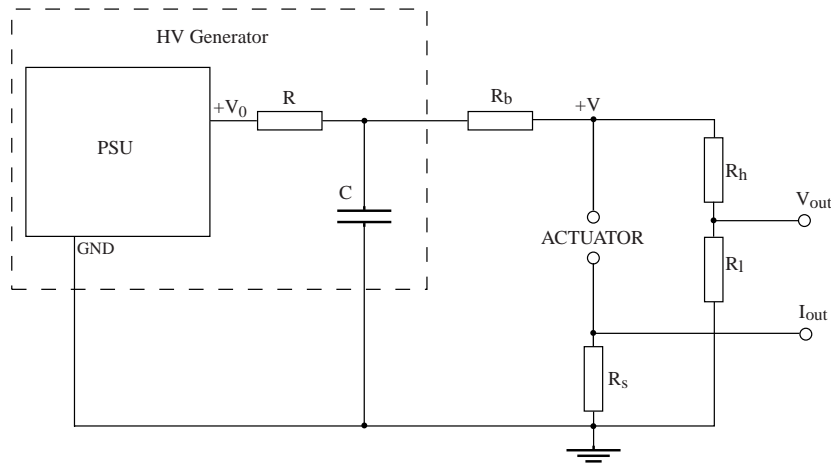


Figure 5: Electric circuit for corona actuators.

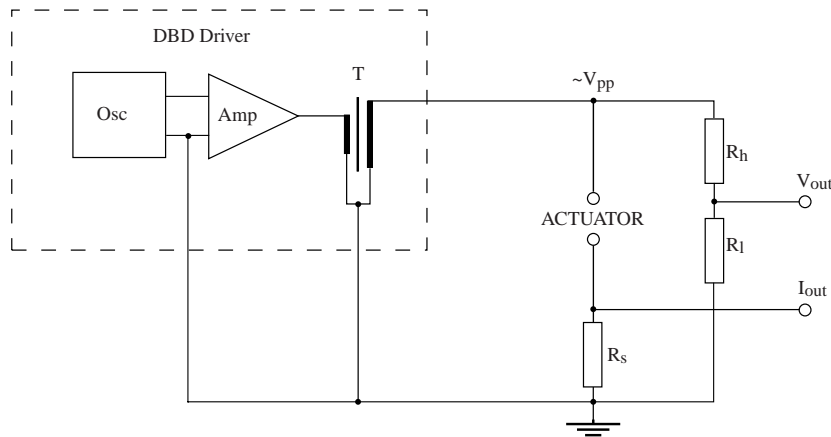


Figure 6: Electric circuit for DBD actuators.

sources in the electrical measurements on the resulting power values gives accuracies in the order of 0.4W (or 1W/m) for the corona set and 1.2W (or 3W/m) for the DBD set.

The ionic wind velocity has been measured by means of a pitot probe made of an insulating composite material, with an outer diameter  $d_o = 0.8\text{mm}$  and an inner one  $d_i = 0.4\text{mm}$ . The probe is connected to a differential pressure transducer (range  $\pm 200\text{ Pa}$ , accuracy  $0.05\text{ Pa}$ ) and aligned with the longitudinal direction  $x$  of the far stream, as sketched in Fig. 7, which represents the setup for corona as well as for DBD actuators. The probe has been moved along two different  $yz$  planes, normal to the stream direction, by means of a traversing system. The measurement planes are located  $x_1 = 17\text{ mm}$  and  $x_2 = 40\text{ mm}$  downstream of the tips line  $x_{tip}$ , as shown in Fig. 7. These positions have been set in order to obtain far field measurements, where the ionic wind direction becomes closer to the  $x$ -direction, whereas the velocity field in the near zone of the tips can have a non negligible three-dimensionality. More precisely, the directional sensitivity of the pitot probe can be expressed by writing the relation involving the flow velocity  $v$ , the measured pressure  $p_m$  and the atmospheric (reference)  $p$  as [14]

$$p_m - p = \frac{1}{2} C_p \rho v^2 \quad (2)$$

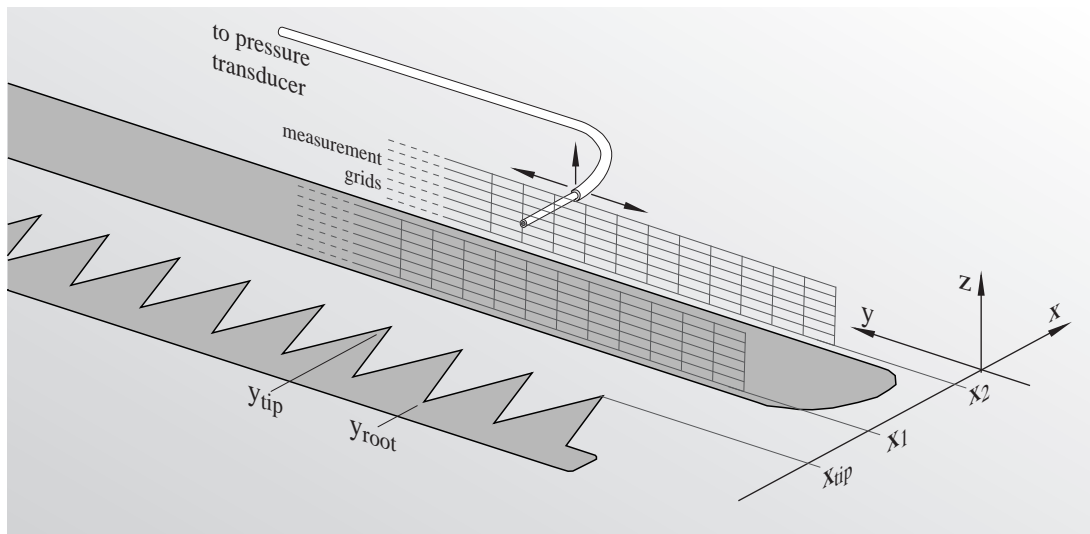


Figure 7: Experimental setup and reference system for total pressure measurements, shown for a corona actuator. The setup for DBD actuators is the same, but the ground electrode is immersed in the dielectric.

where  $\rho$  is the air density and  $C_p$  is a coefficient including the experimental corrections, i.e.  $C_p = 1$  only for a measure carried out under ideal conditions. A misalignment  $\alpha$  between the velocity vector and the axis of this probe ( $d_i/d_o = 0.5$ ) gives a value  $0.99 \leq C_p \leq 1$  within  $\alpha = \pm 17^\circ$  [15, 16], in other words  $C_p$  can be set to 1 obtaining pressure accuracies better than 1% for flow directions within a range of  $34^\circ$  around the probe axis, which is an achievable condition in the far field. Instead, a  $C_p$  value slightly different has been imposed to correct other sources of errors [14], namely the local deviation of the flow when the probe touches the wall and the low Reynolds number of the probe  $Re = d_i v / \nu$  based on the air viscosity  $\nu$  (in the present tests  $Re$  may drop below 50). Both these effects may give errors in the order of few % of the pressure readings, but after the compensation the overall accuracy of pressure has been maintained in the order of 1%. The gas density in Eq. (2) has been determined in each test by the atmospheric pressure and temperature through the state law, assuming that the plasma heating is negligible on the scale of the accuracy for  $\rho$ . The humidity during the tests has been maintained to  $22 \pm 5\%$ . Finally, the uncertainty of the velocities reported in the following results, obtained by propagation through Eq. (2), is always smaller than 0.1m/s; this sets also the uncertainty on the derived quantities as the mass flow, excluding error sources due for example to small irregularities of the electrodes shapes.

### 3 Results

The presentation of the results is introduced here by a photograph of the two kinds of actuators considered in this work, acquired with an exposure of 1s. Fig. 8 shows a corona and a DBD having the same active electrode, in order to recall the definite differences between the two devices when they create a ionic wind. From the image, it is clear that the ionization regions of a multi-tip corona actuator are localized on the tips, so that each one gives rise to an ion drift zone in the downstream region. The ionic wind is then made of periodic jets spreading from the tips with parallel axes and merging downstream. Also in the DBD actuators the tips are regions of high ionization, but the discharge is generated along the whole contour of the active electrode, and the gas velocity is locally normal to the contour line. This gives rise to a gas stream with a three-dimensional structure, well-known in literature for electrodes of periodic shape [7, 9]. In particular, regions between adjacent tips create a vertical component directed away from



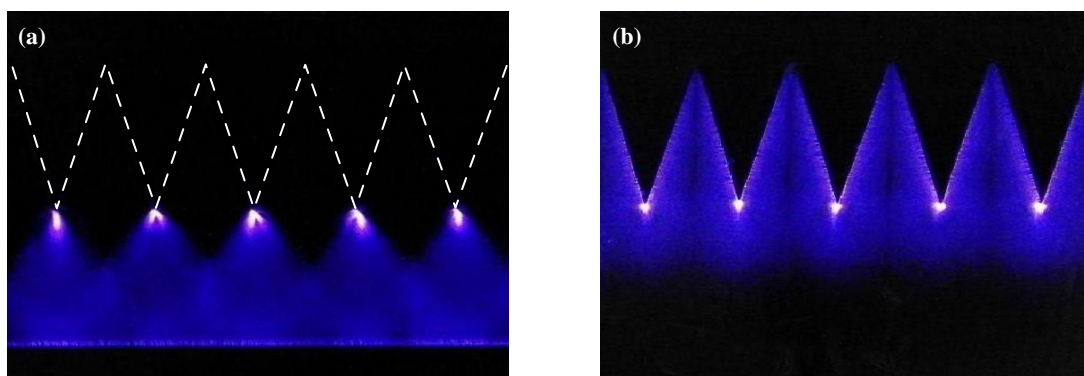


Figure 8: Photograph of working actuators, the corona C5 (a) and the DBD D6 (b). The upstream electrodes have the same geometry  $(n, r) = (100, 1.5)$ , the tips are aligned at the same  $x$  coordinate. The dashed line marks the contour of the corona anode.

the wall, whereas in the regions behind tips the flow moves toward the wall. Thus, a DBD creates a ionic wind made of a longitudinal component interacting with transverse components that produce periodic pinch–spread effects on the streamlines and, accordingly, a distribution of streamwise vorticity. As shown in the following results, this flow structure has effects also on the measurements of the far–field streamwise velocity component.

### 3.1 Electrical measurements

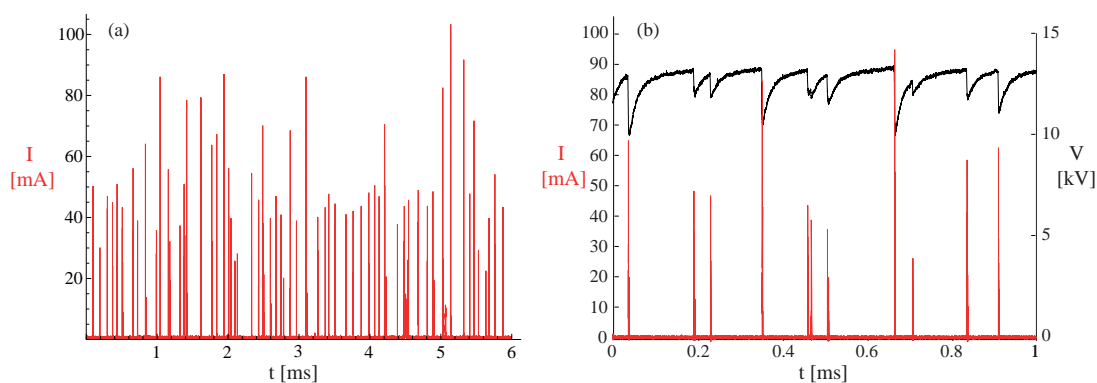


Figure 9: Samples of current (a) and current–voltage (b) time histories for the corona actuator C7.

The electrical characterization of the corona actuators is carried out as in Fig. 5. A sample of the recorded current can be seen in Fig. 9a. This shows that the current is mainly due to repetitive streamers, the relevant pulses have durations in the order of 100ns and heights in the order of 100mA. There is also a small continuous component, generally in the order of 0.3mA. The Fig. 5b shows also a close up of current and voltage over an enlarged time scale, here it is evident that each streamer causes a voltage drop with partial discharge of the capacity of the circuit. It is worth noting that most data about the present corona actuators have been acquired thanks to their improved stability, that appears to be related to the tip sharpness. Actually, the available data show that the occurrence of transient sparks, recordable as short current pulses much larger than streamers, diminishes rapidly as the  $r$  parameter grows.

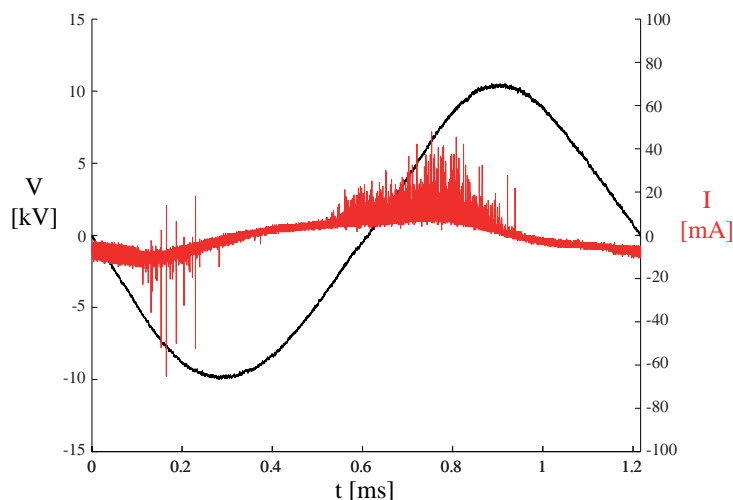


Figure 10: Current–voltage time history over a period for the DBD actuator D13.

Fig. 10 shows analogous recordings of current and voltage over the cycle of a DBD actuator, carried out as in Fig. 6. In this case the curves are similar to the ones widely reported in literature, with numerous streamers appearing in the current signal during the rising phase of the positive half wave in the voltage curve. As usual, the streamers on the opposite half wave are suppressed by the encapsulation of the immersed electrode, with few exceptions.

### 3.2 Ionic wind curves and maps

A first sample of the available data is shown in Fig. 11, that presents two sets of ionic wind curves, representing the velocity profile downstream of a tip at the position  $x_1, y_{tip}$  shown in Fig. 7. Each one is obtained as an average curve over 3 different tips: the typical uncertainty of these curves is in the order of 0.2m/s in Fig. 11a (corona) and 0.1m/s in Fig. 11b (DBD). As explained above in §2, the measurement system has an inherent uncertainty smaller than 0.1 m/s, but this value can be worsened by the small irregularities of the electrodes due to their manufacture technology. The corona actuators are more sensitive to this effect, so that the relevant uncertainty is larger. The Fig. 11a compares 5 corona actuators having the same tip width  $w = 10\text{mm}$  and growing tip heights  $h = 10, 15, 20, 30, 40\text{mm}$  (sharpness  $r = 1...4$ ), including the wire-to-plate actuator C1 as a reference. The multi-tip anodes give a clear velocity increase, slightly dependent on the tip sharpness and saturating for very long tips. At the same time, the velocity maximum is moved away from the wall. The velocity gain can be easily related to the increased tip–cathode field; the position of the velocity maximum could be related to the shape of the electric field, extending into a larger volume above the electrodes when driven by the tips, that set locally a definite divergence to the electric field lines.

The Fig. 11b compares 7 DBD actuators with the same tip width  $w = 10\text{mm}$  and growing tip heights  $h = 3, 5, 10, 15, 20, 30, 35\text{mm}$  (sharpness  $r = 0.3...3.5$ ), including the straight case D1 as a reference. The tip heights vary in the same range of the corona actuators on panel (a). Even in this set the multi-tip electrodes increase the overall velocity, but after an initial increase for growing sharpnesses, the velocity for the longest tips decreases. The velocity increase can be related to the high tip–cathode field, but in this case also the active perimeter of the electrode grows with the tip length, so that a blunt tip generates a wide jet surrounded by oblique components, whereas a sharp tip generates a narrow jet surrounded by strongly transverse components, and distributes the available power over a longer perimeter. The velocity

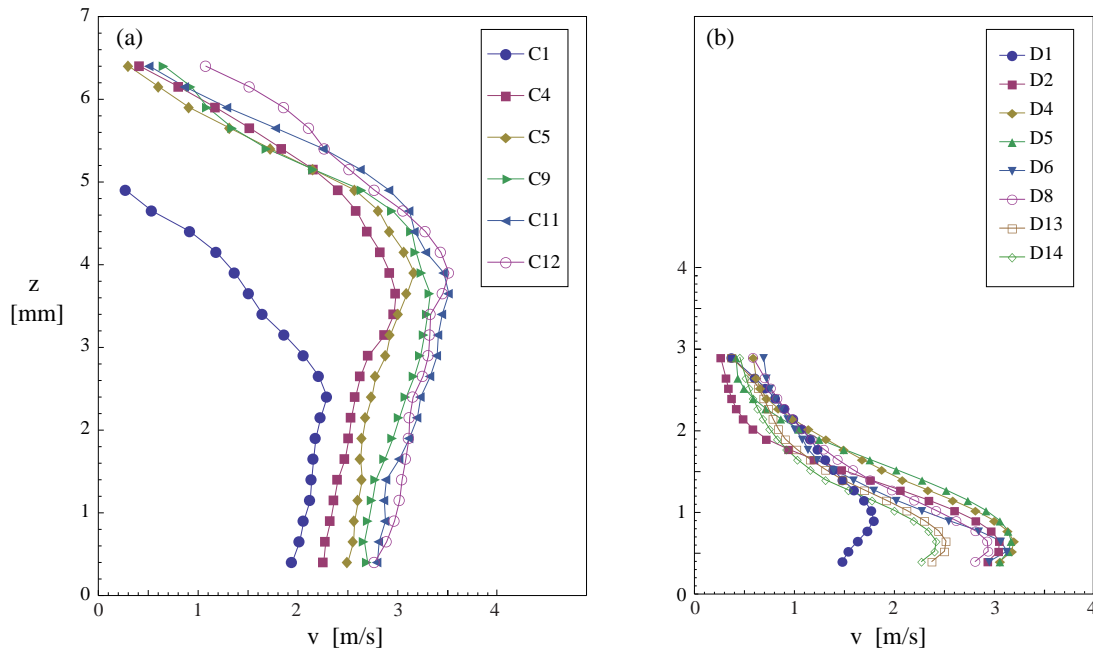


Figure 11: Velocity curves  $v(x_1, y_{tip}, z)$  measured downstream of a tip, for corona (a) and DBD (b) actuators with constant  $w$  and increasing sharpness,  $r = 0 \dots 4$  for C1...C12 and  $r = 0 \dots 3.5$  for D1...D14.

trend shown in figure could arise as a balance between these phenomena, considering that the momentum diffusion while the gas moves from the electrode to the probe is easier in a narrow jet. Another remarkable property for DBDs is the small distance of their velocity maxima from the wall, owing to the shape of the electric field. This distance is always smaller than for coronas. Furthermore, all the multi-tip DBDs move the velocity maximum slightly toward the wall with respect to the straight actuator. This displacement is consistent with a local zone of vertical velocity above each tip.

The vertical positions  $z_{vmax}$  of the velocity maxima in Fig. 11 appear independent on the actuator shape, except the straight ones: actually, this property turns out to hold for the complete sets. In particular, all the multi-tip corona give a  $z_{vmax} = 4 \pm 0.4\text{mm}$  whereas the wire-plate gives  $z_{vmax} = 2.4 \pm 0.25\text{mm}$  and all the multi-tip DBD give a  $z_{vmax} = 0.65 \pm 0.15\text{mm}$  whereas the straight one gives  $z_{vmax} = 0.9 \pm 0.1\text{mm}$ . Finally, it is worth noting that the present setup gives velocities in the same order for the two sets considered. This is a consequence of size, scale and power supply chosen for the two sets, and permits some cross comparisons, as for example the power needed by a corona and a DBD to give a similar ionic wind.

Another kind of measurement achievable with this setup is the velocity field induced by the actuators on planes normal to the ionic wind. Fig. 12 and 13 show the fields induced by the corona C9,  $(n, r) = (100, 2)$ , on the planes located at  $x_1 = 17\text{mm}$  and  $x_2 = 40\text{mm}$  downstream of the tips line  $x_{tip}$ . Slight differences between the tip fields are visible in both maps, due to the manufacture technology of the electrodes. The second map shows the momentum diffusion as the jets created by the tips spread out along their paths. Even at larger distances, the velocity maximum remains quite far from the wall. The mass flow through these planes does not exhibit remarkable differences: by integration, the values referred to the span  $S$  are 49 g/s in Fig. 12 and 54 g/s in Fig. 13, indicating that the latter intercepts slightly more flow than the former but the global alignment of the ionic wind with the longitudinal direction is clear. These velocity maps are representative of the whole set of actuators, since they behave in a similar

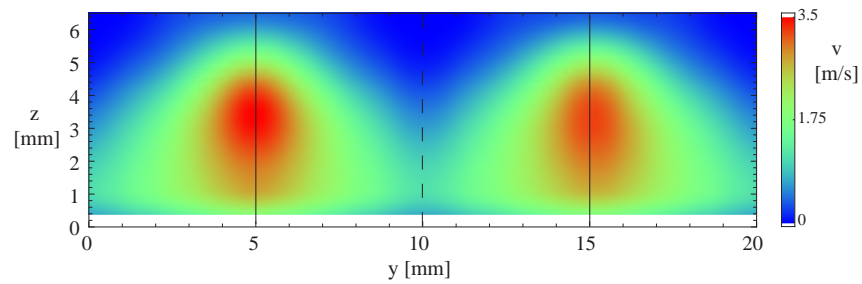


Figure 12: Corona C9, interpolated velocity map  $v(x_1, y, z)$ . Solid lines at  $y_{tip}$ , dashed lines at  $y_{root}$ .

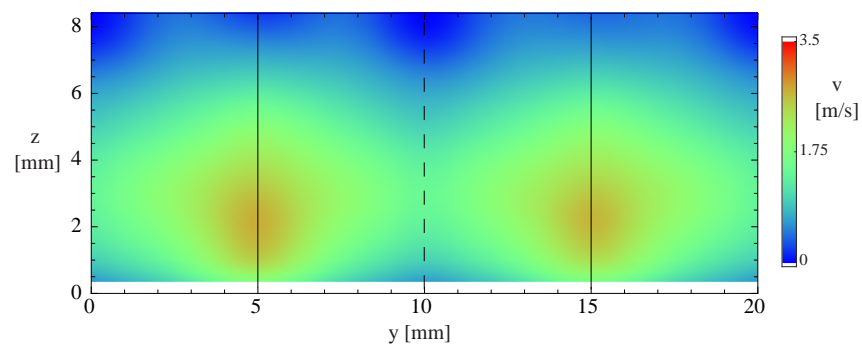


Figure 13: Corona C9, interpolated velocity map  $v(x_2, y, z)$ . Solid lines at  $y_{tip}$ , dashed lines at  $y_{root}$ , velocity scale as in Fig. 12.

way in the ionic wind generation, excluding the dependence on the tip scale.

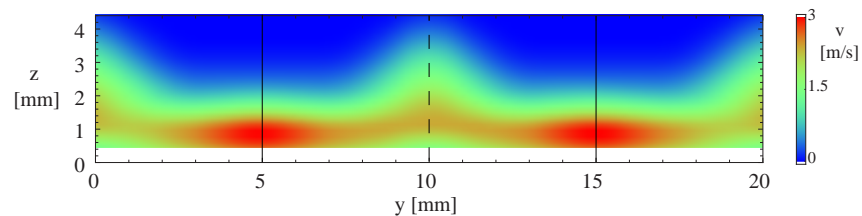


Figure 14: DBD D8, interpolated velocity map  $v(x_1, y, z)$ . Solid lines at  $y_{tip}$ , dashed lines at  $y_{root}$ .

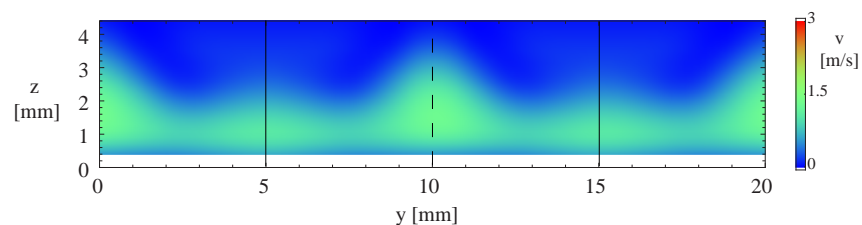


Figure 15: DBD D8, interpolated velocity map  $v(x_2, y, z)$ . Solid lines at  $y_{tip}$ , dashed lines at  $y_{root}$ , velocity scale as in Fig. 14. The local velocity maximum is aligned with  $y_{root}$ .

Fig. 14 and 15 show the velocity fields induced by the DBD D8, having the same upstream electrode as corona C9, on the planes at  $x_1, x_2$ . Comparing Fig. 14 with the corona case at  $x_1$ , the longitudinal velocities are in the same order, and the velocity maxima are closer to the wall, but in this case the 3D effects are evident: besides the local maxima centered on the tip coordinates  $y_{tip}$ , there are regions of non negligible velocity corresponding to  $y_{root}$ , extended over high  $z$  values. This is the effect of the vertical velocity always generated in the valley between adjacent tips, which has a lifting effect on the longitudinal component. At the larger downstream distance  $x_2$ , the map of Fig. 15 shows another phenomenon appearing only in the DBD gas streams: owing to the streamlines pinching over the root zones and spreading over the tip zones, at  $x_2$  the streamlines of higher velocity coalesce over the root coordinate  $y_{root}$  (here is the maximum of the map), whereas the field of motion at  $y_{tip}$  is weakened. In literature, this effect has been described for sinusoidal [7, 17] and serrated [18] electrodes. The flow topology visible in these velocity maps is very similar even for the other DBDs with sharp tips (high  $r$ ) and similar width  $w$ . It is likely to occur as a general property, but the  $x$  distance necessary to develop the flow from the pattern of Fig. 14 to the one of Fig. 15 seems to depend on the periodicity  $n$  of the actuators, so that a complete investigation would require a further modification of the setup, exploring the velocities at several downstream distances  $x_i$ .

### 3.3 Comparisons in the parameter space

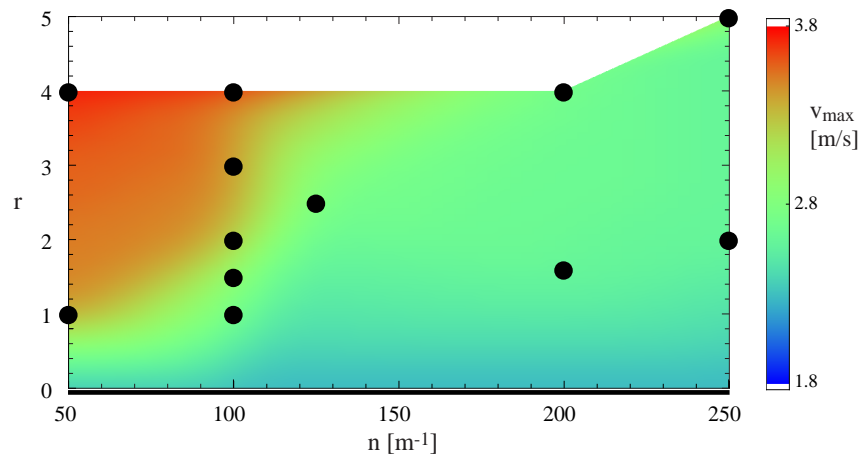


Figure 16: Corona set: maximum velocity along the parameter plane,  $v_{max}(n, r)$  measured at  $x = x_1$ .

This section contains compared measurements performed over the complete corona and DBD sets, presenting the results in the parameter space  $(n, r)$  defined by Eq. (1). All the measured quantities are reported by means of spline-interpolated surfaces plotted over the relevant domains in the  $(n, r)$  space. This method has been chosen instead of presenting tables of data because of its easier readability, however the data point density corresponding to the selected electrode shapes is inhomogeneous, thus the visible surfaces should be taken mainly as a guide to evaluate the actual data values.

Fig. 16 and 17 show the maximum velocity  $v_{max}(n, r)$  recorded along the parameter plane for the corona and DBD sets at  $x = x_1$  (for each actuator, this velocity is always found at  $y_{tip}$  and at a given  $z$  height, lower for the DBD). In these and in the following figures, the actuators under test are represented by dots superimposed to the map, except the straight one, which is represented by the thick line  $r = 0$ . Within the corona set, the highest velocity in Fig. 16 has been recorded for the actuator C13 (50,4), which has sharp separate tips and a very high local electric field. This point lies on the map border,

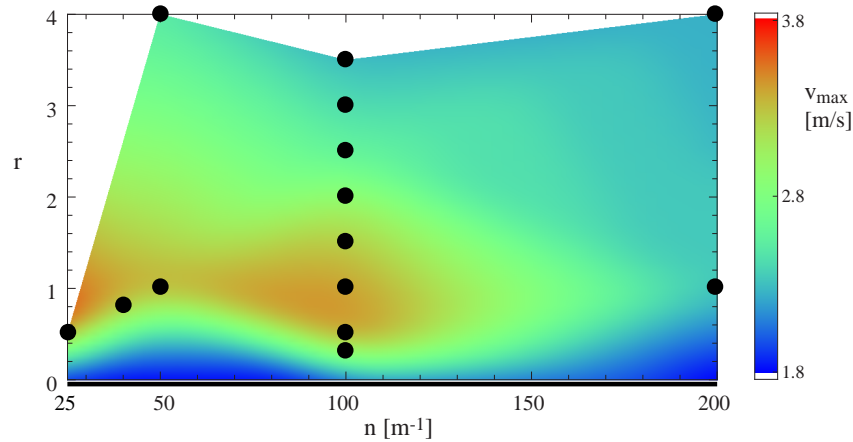


Figure 17: DBD set: maximum velocity along the parameter plane,  $v_{max}(n, r)$  measured at  $x = x_1$ . Velocity scale as in Fig. 16.

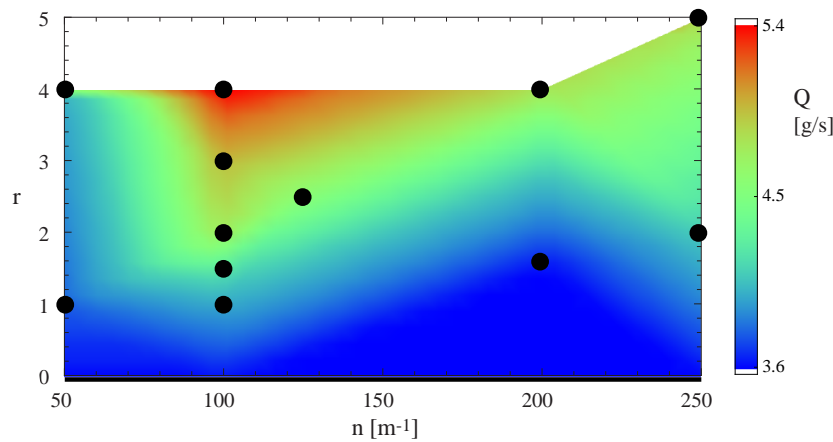


Figure 18: Corona set: mass flow  $Q(n, r)$  measured at  $x = x_1$ .

indicating that even larger local velocities could be achieved. Within the DBD set, the highest velocities in Fig. 17 have been recorded for the actuators D11 (25,0.5) and D5 (100,1), with similar values in the neighborhood, a zone ranging approximately from  $r = 0.5$  to 1 and  $n = 25$  to 100. As described in §3.2 for a subset of the available DBDs, here the tip sharpness is enough to increase the longitudinal velocity but not so high as to create a very long electrode perimeter, that may consume a remarkable power even in the creation of transverse velocity components. But this map shows that  $v_{max}$  also decreases for high  $n$  at constant  $r$  (constant perimeter), suggesting that the advantages due to the high local field on a tip are reduced when the tips are too close each other.

A global quantity that may give information on the ability to produce a longitudinal ionic wind is the mass flow generated by an actuator through a normal plane. Fig. 18 and 19 show the mass flows  $Q(n, r)$  for the corona and DBD sets measured at  $x = x_1$  over planes of span  $S$  and vertical ranges as in Fig. 12 and 14. Within the corona set, the highest flow is registered for the actuator C12 (100,4), characterized by tips sharp but not so numerous. It is likely that, keeping a similar sharpness and increasing  $n$ , the ionization regions become too close each other leading to an electric field more similar to the wire-plate,

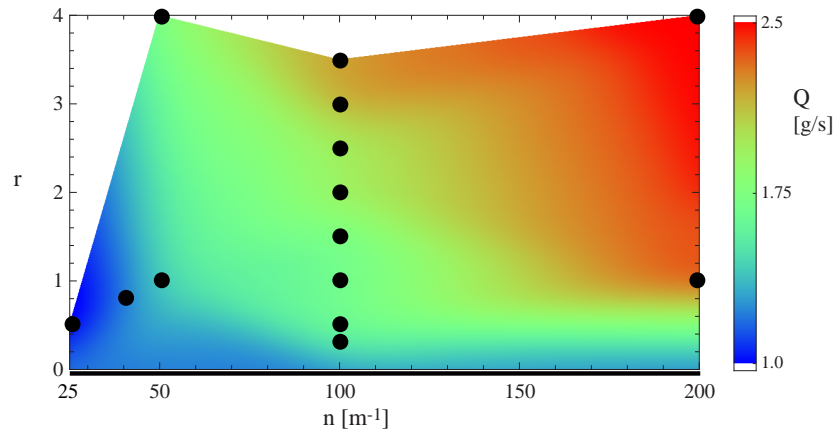


Figure 19: DBD set: mass flow  $Q(n, r)$  measured at  $x = x_1$ .

thus losing the advantages of the multi-tip configuration. Within the DBD set, the highest flow is found on the right border of the map, at the actuator D7 (200,4). In this case the proximity of the tips, even if reduces the value of  $v_{max}$  as seen in Fig. 17, does not impact negatively on the mass flow as for the high- $n$  corona actuators. The reason for the high  $Q$  of this actuator and of the D3 (200,1) can be found by examining the velocities profiles along the whole perimeter: actually, in these high- $n$  DBDs the velocity curves  $v(x_1, y_{root}, z)$  downstream of roots reach values close to the curves  $v(x_1, y_{tip}, z)$  downstream of tips, giving an integral mass flow of high value. For lower  $n$  instead the velocity field has large variations along the  $y$  axis, leading to lower  $Q$  values.

### 3.4 Power and efficiency in the parameter space

Another field of comparison for the actuators is defined by their power consumption and mechanical performance. According to the electric setup of Fig. 5 and 6, the average electric power consumption can be calculated as

$$W_e = \frac{1}{T} \int_0^T V(t)I(t) dt \quad (3)$$

where  $T$  is a finite number of cycles in a DBD and a time much longer than the streamer scale in a corona. Considering the longitudinal ionic wind, the relevant mechanical power can be written as a kinetic energy flow rate through a measurement plane of span  $S$ :

$$W_m = \frac{1}{2} \rho \int_S \int_0^{z_{max}} v(y, z)^3 dy dz . \quad (4)$$

Here the velocity is intended as the steady value obtained through Eq. (2) from the pitot probe, that works with the transducer and the connecting line as a low pass hydraulic system of very low cut frequency [16], in the order of 0.5Hz.

A meaningful quantity for the actuators is the electric power per unit length  $W_e/S$ : for the corona set, this quantity exhibits a rapid decrease as the sharpness  $r$  changes from 0 to a finite value, then becomes nearly constant. More precisely, the wire-plate actuator C1 requires 105W/m (this value could be affected by the small span of C1, but it is likely to remain quite high even when corrected for the end effects); instead, all the multi-tip actuators have low and very similar values, almost independent on the parameters  $n, r$ , with a mean value of  $16.0 \pm 1.5$ W/m. The relevant map for  $W_e/S$  would appear as a

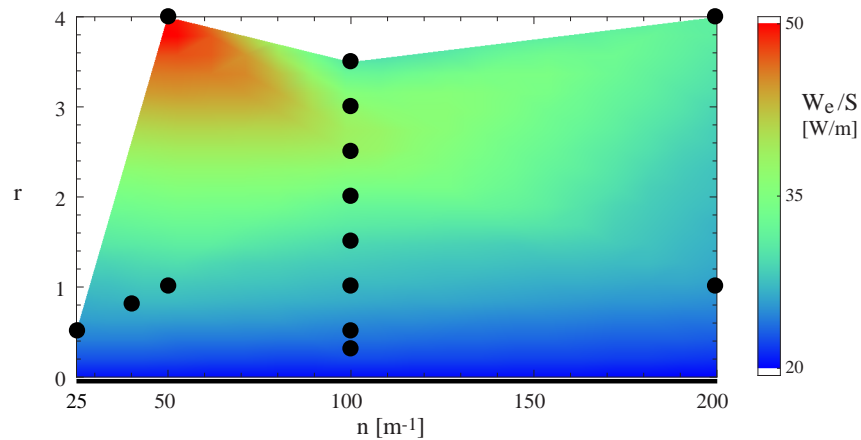


Figure 20: DBD set: electric power/area ratio.

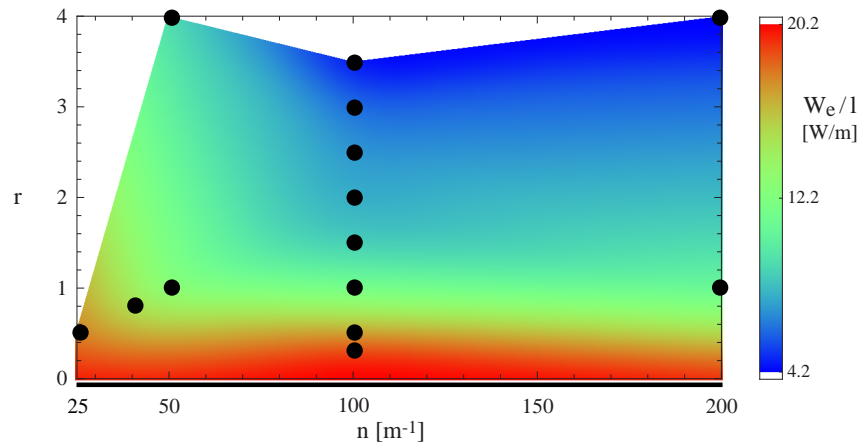


Figure 21: DBD set: electric power/perimeter ratio.

flat surface, except a rise along the axis  $r = 0$ . For the DBD set, the values of  $W_e/S$  are reported in Fig. 20, here the power increases weakly with the tip sharpness, and the maximum value corresponds to the actuator D15 (50,4), which has separate tips. Another interesting quantity for the DBD set is the electric power referred to the active length  $W_e/l$ , where the ratio is calculated over the active perimeter  $l$  of the upstream electrode, because in a DBD the entire contour of the tips takes part in the plasma production. This quantity is shown in Fig. 21, here the maximum value is recorded for the straight actuator D1, which has the shortest active perimeter.

Finally, the normalized power of the ionic wind can be presented by means of the electromechanical efficiency [1, 19]

$$\eta = \frac{W_m}{W_e}. \quad (5)$$

Fig. 22 shows the  $\eta$  values for the corona set. The maximum value in this figure corresponds to the highest mass flow of Fig. 18, i.e. the actuator C12 (100,4), but in general this map reveals that the efficiency increases with the tip sharpness, particularly for moderate  $n$  values. As for the mass flow map, it is



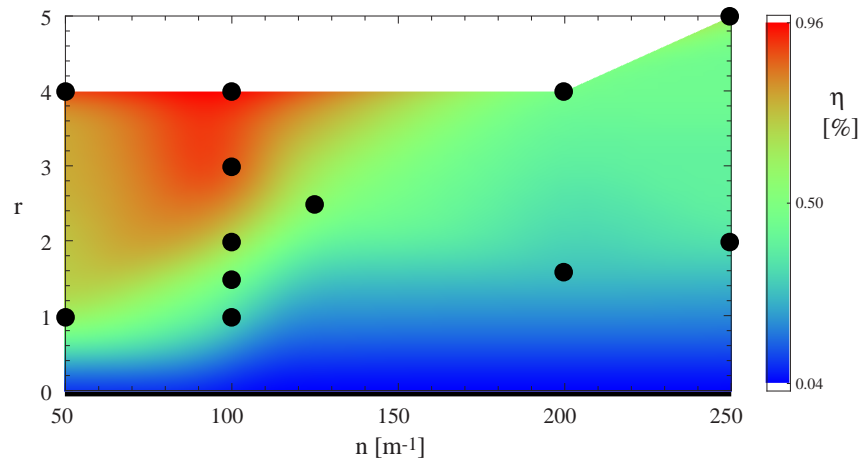


Figure 22: Corona set: electromechanical efficiency.

likely that tips too numerous worsen the performance of the actuator, leading to an electric field more similar to the wire–plate case, because of the mutual proximity of the ionization regions. Fig. 23 shows the  $\eta$  values for the DBD set, here the most efficient devices are the D4 (100,0.5) and the D3 (200,1), with similar  $\eta$  values that stem from different properties. In fact, D4 belongs to the optimal region for  $v_{max}$  (Fig. 17) and D3 to the region of high  $Q$  (Fig. 19). It is important noting that the DBD values are all definitely lower than the corona values, but the present definition of  $\eta$ , while appropriate to the present study, accounts only for the efficiency in producing a given mass flow longitudinally oriented. In other words, this parameter can account neither the vertical ( $z$ ) position of the velocity maximum, nor the transverse velocity components, all important in influencing the shape of a boundary layer in flow control problems.

## 4 Conclusions

In this experiment, two sets of multi-tip actuators (13 coronas and 15 DBDs) have been tested on the basis of the far-field longitudinal ionic wind produced by each device. Their upstream electrodes have contours provided with periodic triangular tips, the geometry is set by the tip number per unit length  $n$  and the tip sharpness  $r$  (height/width ratio), that define a parameter space  $(n, r)$ . Sizes, gaps of the electrodes and power supplies are chosen to give comparable velocities for the two sets considered, in order to permit cross comparisons between the two kinds of actuators. As references, a corona and a DBD of straight geometry have been included among the devices under test.

The effects of the triangular tips on the upstream electrodes can be summarized as follows, with respect to the reference (straight) cases:

- The stability of corona actuators grows with the tip sharpness  $r$ , the undesired transient sparks become rare for high  $r$  values.
- The flow pattern for corona actuators is an array of jets spreading from the tips and merging at large distances. Also for DBD actuators, the longitudinal far flow appears as made of jets, but they may be aligned with tips as well as with roots, because of the three-dimensional generation of the flow at the electrode contour, where transverse motions are present. Actually, as known in the literature, the gas may shift transversally and rotate while it moves downstream, and the effects are clearly visible even by the present measurement method.

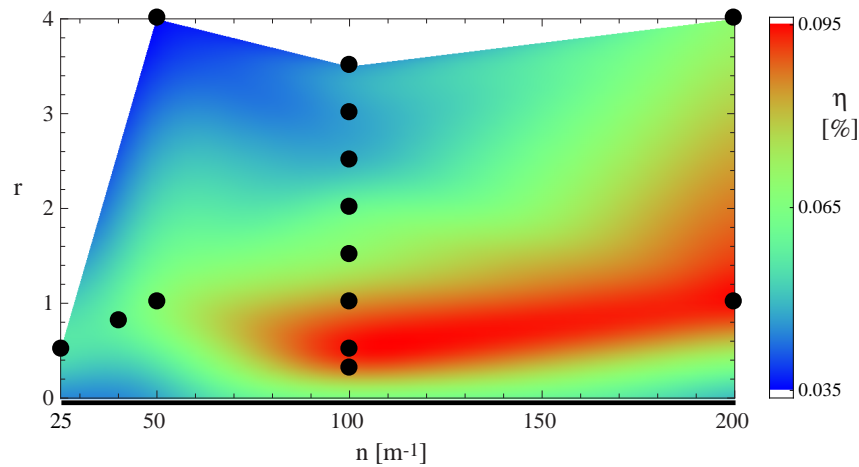


Figure 23: DBD set: electromechanical efficiency.

- The longitudinal ionic wind for coronas increases strongly downstream of the tips and decreases downstream of the roots. High velocities are recorded downstream of the tips also for the DBDs, but in this case there are further zones of high velocity even downstream of the roots, because of the transverse components.
- The vertical scale of the flow grows for coronas, and the local velocity maxima move away from the wall. The local maxima for the DBDs move toward the wall when aligned with the tips, the opposite when aligned with the roots.

The evaluations along the parameter plane  $(n, r)$  have been performed over similar regions, namely  $50 \leq n \leq 250, 0 \leq r \leq 5$  for the corona set and  $25 \leq n \leq 200, 0 \leq r \leq 4$  for the DBD set. The results have been plotted as maps and can be outlined as follows:

- The maximum local velocity within the corona set is given by an actuator with very sharp and separate, not numerous tips, on the map border. The maximum local velocity within the DBD set is given by an actuator with moderately sharp and numerous tips, in a region of the plane where other actuators give similar values. This can be considered an optimal region for the longitudinal ionic wind.
- The largest mass flow for coronas has been recorded for high sharpness and moderate tips number. It is definitely larger than the maximum mass flow in the DBD set, that is located at the map border and corresponds to high  $r$  and  $n$  at the same time.
- The power consumption per unit length appears as constant for multi-tip coronas, but much lower than for a straight actuator. The power per unit length of DBDs grows with tip sharpness and is maximum for the actuator with sharp and separate tips, on the map border. The power consumption for the DBD set can also be normalized over the active electrode perimeter, in this case the maximum value corresponds to the straight actuator.
- The electromechanical efficiency of multi-tip coronas in producing the ionic wind is definitely better than for a wire-plate corona. It grows rapidly with sharpness, particularly for moderate values of  $n$ . The efficiency of DBDs exhibits optimal points within the region under study, but is always much lower than for coronas.

Globally, the present work shows that actuators provided with multiple tips have better performances in producing a longitudinal ionic wind. In particular, it may suggest new uses for corona actuators in flow control problems, whereas it may provide new information about the performances of DBD actuators having this geometry. The direct comparison of multi-tip coronas and DBDs in producing a given ionic wind shows that the former are much more efficient than the latter. However, a multi-tip DBD can interact with a boundary layer in different ways, by local acceleration and/or vortex generation at the same time: the complete characterization of the generated flow as a function of the electrode geometry, beyond the scope of the present work, should be object of further studies.

## References

- [1] E. Moreau, Airflow control by non-thermal plasma actuators, *J. of Physics D: Applied Physics*, 40(3) (2007), 605–636.
- [2] T.C. Corke, C.L. Enloe, S.P. Wilkinson, Dielectric barrier discharge plasma actuators for flow control, *Annual Rev. of Fluid Mech.* 42 (2010) 505–529.
- [3] J.J. Wang, K.S. Choi, L.H. Feng, T.N. Jukes, R.D. Whalley, Recent developments in DBD plasma flow control, *Prog. Aerosp. Sci.* 62 (2013) 52–78.
- [4] N. Benard, E. Moreau, Electrical and mechanical characteristics of surface AC dielectric barrier discharge plasma actuators applied to airflow control, *Exp. Fluids* 55:1846 (2014)
- [5] T. Abe, Y. Takizawa and S. Sato, Experimental Study for Momentum Transfer in a Dielectric Barrier Discharge Plasma Actuator, *AIAA J.* 46(9) (2008), 2248–2256.
- [6] F.O. Thomas, T.C. Corke, M. Iqbal, A. Kozlov and D. Schatzman, optimization of dielectric barrier discharge plasma actuators for active aerodynamic flow control, *AIAA J.* 47(9) (2009) 2169–2178.
- [7] C.C. Wang, R. Durscher and S. Roy, Three-dimensional effects of curved plasma actuators in quiescent air, *J. Appl. Phys.* 109, 083305 (2011).
- [8] A. Berendt, J. Podlinski and J. Mizeraczyk, Comparison of airflow patterns produced by DBD actuators with smooth or saw-like discharge electrode, *J. of Physics: Conference Series* 301(1): 012018, IOP Publishing (2011).
- [9] R. Joussot, A. Leroy, R. Weber, H. Rabat, S. Loyer and D. Hong, Plasma morphology and induced airflow characterization of a DBD actuator with serrated electrode, *J. of Physics D: Applied Physics* 46(12): 125204 (2013).
- [10] L. Leger, E. Moreau, G. Touchard, Effect of a DC Corona Electrical Discharge on the Airflow Along a Flat Plate, *IEEE Trans. Industry Appl.* 38(6) (2002) 1478–1485.
- [11] C. Louste, E. Moreau, G. Touchard, Influence of an insulating flat plate on a DC surface corona discharge at various air relative humidities, *Electrostatics 2003: Proceedings of the Electrostatics Conference of the Institute of Physics held in Edinburgh, UK, 2327 March 2003.*
- [12] G. Artana, J. DAdamo, L. Leger, E. Moreau, G. Touchard, Flow Control with Electrohydrodynamic Actuators, *AIAA J.* 40(9) (2002) 1773–1779
- [13] J. Kriegseis, B. Möller, S. Grundmann, C. Tropea, Capacitance and power consumption quantification of dielectric barrier discharge (DBD) plasma actuators, *J. of Electrostatics* 69 (2011) 302–312
- [14] C. Tropea, A.L. Yarin, J.F.Foss (Eds.), *Springer Handbook of Experimental Fluid Mechanics*, Springer–Verlag (2007) Section 5.1.1
- [15] S.H. Chue, Pressure probes for fluid measurement, *Prog. Aerosp. Sci.* 16 (1975) 147–223
- [16] T. Arts, H. Boerigter, M. Carbonaro, J.M. Charbonnier, G. Degrez, D. Olivari, M.L. Riethmuller, R.A. Van den Braembussche, *Measurement techniques in fluid dynamics. An introduction*, Von Karman institute for fluid dynamics, Rhode-Saint-Genese (2001), section 3.2.1

- [17] S. Roy, C.C. Wang, Bulk flow modification with horseshoe and serpentine plasma actuators, *J. Phys. D: Appl. Phys.* 42 (2009) 032004
- [18] Z. Liu, L.Wang, S. Fu, Study of flow induced by sine wave and saw tooth plasma actuators, *Science China* 54(11) (2011) 2033-2039
- [19] J. Pons, E. Moreau, G. Touchard, Asymmetric surface dielectric barrier discharge in air at atmospheric pressure: electrical properties and induced airflow characteristics, *J. Phys. D: Appl. Phys.* 38 (2005) 3635-3642